Scientific paper

Structural investigations of the XeF_2–PtF_5 system: crystal structures of $[Xe_2F_3][PtF_6]\cdot XeF_2$, $[Xe_2F_3][PtF_6]$, and $[XeF][PtF_6]$

Klemen Motaln[1,2] and Matic Lozinšek*[,1,2]

[1] *Extreme Conditions Chemistry Laboratory (ECCL K2), Jožef Stefan Institute, Jamova cesta 39, 1000 Ljubljana, Slovenia*

[2] *Jožef Stefan International Postgraduate School, Jamova cesta 39, 1000 Ljubljana, Slovenia*

* *Corresponding author: E-mail: matic.lozinsek@ijs.si*

Received: 02-06-2026

Dedicated to the memory of Prof. Dr. Boris Žemva (1940–2023), whose passion for noble-gas chemistry was infectious and inspired our work in this fascinating field.

Abstract

The XeF_2–PtF_5 system was reinvestigated by exploring reactions in either anhydrous HF or at elevated temperatures. This approach enabled the structural characterization of four members of the system, namely $[Xe_2F_3][PtF_6]\cdot XeF_2$(*mC*120), $[Xe_2F_3][PtF_6]\cdot XeF_2$(*oP*120), $[Xe_2F_3][PtF_6]$, and $[XeF][PtF_6]$(*mP*108), by means of single-crystal X-ray diffraction and low-temperature Raman spectroscopy.

Keywords Noble-gas compounds; xenon(II); platinum(V); fluorides; single-crystal X-ray diffraction

1. Introduction

Owing to its commercial availability and relative ease of handling, XeF_2 remains the most extensively studied and widely used noble-gas compound.[1] It is a moderately strong fluoride-ion donor, and studies of its reactions with Lewis-acidic pentafluorides AF_5 (e.g., A = As, Sb, Bi, V, Nb, Ta, Ru, Os, Rh, Ir, Pt, Au) have shown that such systems predominantly yield phases with three stoichiometries, namely 2:1, 1:1, and 1:2.[2–8] Structural investigations have established that the 2:1 phases are ionic, comprising discrete V-shaped $[Xe_2F_3]^+$ cations and octahedral $[AF_6]^-$ anions, and are formulated as $[Xe_2F_3][AF_6]$.[2,9] The 1:1 and 1:2 stoichiometry phases have molecular structures comprising tight ion pairs formulated as $[XeF][AF_6]$ and $[XeF][A_2F_{11}]$, respectively, in which the coordinated XeF_2 units exhibit substantial ionization.[10–12] Investigations of the reactions between XeF_2 and platinum-group metal pentafluorides, namely RuF_5, RhF_5, OsF_5, IrF_5, and PtF_5, in BrF_5 solvent indicated that, for each of the three stoichiometries, the corresponding compounds form isomorphous series across the platinum-group metals.[2,3] To date, however, only a limited subset of their crystal structures has been reported, including $[XeF][RuF_6]$,[13] $[XeF][IrF_6]$,[14] $[Xe_2F_3][RuF_6]$, $[Xe_2F_3][IrF_6]$, and $[Xe_2F_3][RuF_6]\cdot XeF_2$.[15] Consequently, structural investigations of these systems remain incomplete, which is particularly notable in the case of the XeF_2–PtF_5 system, given the historical relevance of these compounds.

The investigations that followed the preparation of the first noble-gas compound $XePtF_6$ ($XeF_2\cdot PtF_4$),[16] revealed that reaction of Xe with a large excess of PtF_6 yields a material with a stoichiometry close to $Xe(PtF_6)_n$ ($n \approx 2$), containing pentavalent platinum.[17] The powder X-ray diffraction (PXRD) pattern of this material was later revealed to match that of $[XeF][PtF_6]$ prepared from the reaction of XeF_2 with PtF_5 in BrF_5 solvent.[3] Moreover, it was revealed that upon warming $Xe(PtF_6)_n$ ($n \approx 2$) above 60 °C, the product became more friable and identified by diffraction pattern as $[XeF][Pt_2F_{11}]$, implying that the original $Xe(PtF_6)_n$ ($n \approx 2$) material consists of $[XeF][PtF_6]$ and amorphous PtF_5.[3,18] Subsequently, it was demonstrated that molten XeF_2 can oxidize PtF_4 to yield $[Xe_2F_3][PtF_6]$, which can in turn be decomposed by heating to 70 °C under dynamic vacuum to give $[XeF][PtF_6]$. Both compounds were characterized by vibrational spectroscopy and powder X-ray diffraction.[19]

In the present study, the XeF_2–PtF_5 system was reinvestigated, resulting in the crystal structure determination of two polymorphs of $[Xe_2F_3][PtF_6]\cdot XeF_2$, as well as $[Xe_2F_3][PtF_6]$, and $[XeF][PtF_6]$(*mP*108). These results establish the XeF_2–PtF_5 family as one of the more comprehensively explored among XeF_2–AF_5 systems and provide detailed crystallographic data for compounds that are among the earliest reported examples of noble-gas chemistry.

2. Experimental

Caution: Handling of anhydrous HF (aHF), F_2, and strongly-oxidizing fluorides requires great care and should be conducted only in a well-ventilated fume hood by appropriately trained personnel. It is imperative that suitable personal protective equipment is worn at all times and that access to proper treatment procedures is available in case of exposure.[20–22]

2.1. General experimental procedures

A previously described fluorine-resistant vacuum line was used for work involving F_2 or aHF.[23] Solid materials were handled in a nitrogen-atmosphere glovebox (Vigor SG1200/750E), with moisture levels consistently maintained below 1 ppm. Thermal reactions were performed in PTFE-gasketed nickel reactors equipped with nickel valves. Reactions involving the use of aHF solvent were conducted in vessels constructed from fluorinated ethylene propylene copolymer (FEP) tubing, heat-flared at one end and heat-sealed at the other, and capped with brass-encased PTFE valves. Modified, h-shaped FEP reactors[24] were used for crystallization experiments involving the evaporation of aHF induced by a temperature gradient. These reactors were constructed from two FEP tubes, one straight and one bent at 90°, both connected to the valve via a brass-encased PTFE T-junction and male-to-male connectors. Prior to use, all reaction vessels were passivated overnight with 300–600 Torr of F_2.

2.2. Reagents

F_2 (Solvay Fluor, 98–99%) and Pt powder (Thermo Scientific, 99.98%) were used as supplied. Commercial HF (Linde, 99.995%) was condensed into a FEP vessel loaded with K_2NiF_6 (Advance Research Chemicals, 99.9%) and stirred overnight to eliminate residual traces of moisture. XeF_2 was synthesized via a gas-phase photochemical reaction between UV-photolyzed F_2 and Xe, as previously described.[25]

PtF_5 was synthesized by static fluorination of Pt powder enclosed in a nickel pressure vessel, as outlined previously.[26] Approximately 4 bar of F_2 was introduced into a reactor containing Pt powder at ambient temperature, corresponding to an F_2:Pt molar ratio of 3.5–2.8:1, and the mixture was then maintained at 350 °C for 8 hours. The reactor was subsequently recharged with F_2 and heated again to the same temperature. This procedure also generated some volatile PtF_6, which was readily removed under dynamic vacuum, leaving the non-volatile, deep-red PtF_5 adhering to the reactor walls. $RbPtF_6$ was prepared by UV irradiation of a mixture of Pt and RbF in aHF solvent in the presence of a slight excess of F_2, following the procedure previously employed for the synthesis of $CsPtF_6$.[27]

2.3. Synthesis and crystallization

2.3.1. $[Xe_2F_3][PtF_6]\cdot XeF_2$(*mC*120)

In a typical experiment, $nXeF_2\cdot PtF_4$ ($1 < n < 1.6$) (178 mg), obtained by the interaction of XeF_2 with Pt powder in aHF,[28,29] was loaded into a nickel reactor together with XeF_2 (188 mg, 1.11 mmol). The reactor was then placed in an oven at 130 °C for 22 hours. The reactor was then removed from the oven and allowed to cool to room temperature. Inspection of the reactor contents revealed the formation of a bright-yellow powder together with larger yellow crystals suitable for single-crystal X-ray diffraction (SCXRD) analysis.

2.3.2. $[Xe_2F_3][PtF_6]\cdot XeF_2$(*oP*120)

XeF_2 (80 mg, 0.473 mmol) was added to an h-shaped FEP reaction vessel containing $RbPtF_6$, which had been synthesized photochemically from Pt (30 mg, 0.154 mmol), RbF (16 mg, 0.153 mmol), and an excess of F_2. aHF solvent (1.4 mL) was then added, forming a bright orange-yellow solution with an insoluble yellow precipitate remaining at the bottom of the main arm. The clear yellow supernatant was decanted into the side arm of the reactor, which was subsequently placed in a thermostated cooling bath, with the main arm submerged in chilled EtOH. The temperature gradient between the two arms was increased from 4 to 16 °C over two days, facilitating the crystal growth. SCXRD analysis of the yellow crystals from the side arm identified them as $[Xe_2F_3][PtF_6]\cdot XeF_2$(*oP*120) and $RbPtF_6$. The Raman spectrum of the yellow precipitate from the main arm showed only bands attributable to $RbPtF_6$.

2.3.3. $[Xe_2F_3][PtF_6]$

A nickel reaction vessel containing $[Xe_2F_3][PtF_6]\cdot XeF_2$(*mC*120), prepared as described above, was connected to the vacuum line via a U-shaped FEP trap immersed in liquid nitrogen and pumped under dynamic vacuum for a period of 9 hours, until the accumulation of XeF_2 in the trap ceased. The resulting yellow powder was transferred to an FEP reactor and dissolved in aHF. The solution was then gradually cooled to −60 °C in an EtOH bath, during which the precipitation of small yellow crystals was observed. The solvent was removed under dynamic vacuum at −50 °C.

2.3.4. [XeF][PtF_6](*mP*108)

PtF_5 (21 mg, 0.072 mmol) and XeF_2 (6 mg, 0.035 mmol) were weighed into the main arm of an h-shaped FEP reactor, and aHF (1 mL) was condensed onto the solids. The mixture was stirred overnight, resulting in the formation of a yellow solution above a smaller amount of yellow powder precipitate. The solution was decanted into the side arm, and crystal growth was induced by solvent evaporation in a cooling bath thermostat. As soon as the temperature gradient between the two arms exceeded 7 °C, long needle-shaped crystals (> 2 cm in length) of [XeF][PtF_6](*mP*108) precipitated from the solution (Figure 1).

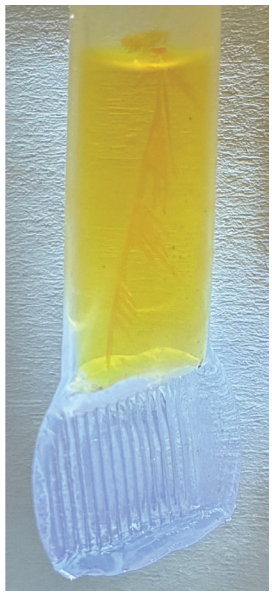

Figure 1. Needle-shaped crystals of [XeF][PtF_6](*mP*108) growing from an aHF solution contained in an FEP tube (6 mm internal diameter; 8 mm outer diameter).

2.3.5. [XeF][PtF_6](*mP*36)

XeF_2 (6 mg, 0.035 mmol) and PtF_5 (24 mg, 0.083 mmol) were loaded into a 6 mm i.d. FEP reactor under N_2 atmosphere. The lower portion of the FEP tube containing the reactants was heat-sealed, and the resulting FEP ampoule was placed in a larger FEP vessel, containing dry N_2 atmosphere. The vessel with the ampoule was then placed in an oven preheated to 70 °C and held at this temperature for 2 hours, after which the oven was gradually cooled by 2 °C/h, until it reached 40 °C. Analysis of the ampoule contents revealed only poorly crystalline [XeF][PtF_6](*mP*36) and its Raman spectrum showed signals belonging to the starting PtF_5 and [XeF][PtF_6].

2.4. Single-crystal X-ray diffraction

Crystalline samples were placed on a watch glass and covered with inert perfluorodecalin oil (ABCR, AB102850, 98%, *cis* and *trans*) inside an inert-atmosphere glovebox. Suitable crystals were selected under a polarized-light stereomicroscope outside the glovebox and mounted on the tip of a MiTeGen dual-thickness polymer loop using Baysilone paste (Bayer-Silicone, mittelviskos). The pin assembly was then grasped with cryo-pin tongs cooled to −196 °C and rapidly transferred to the goniometer head of the diffractometer, where the crystal was protected by a cold nitrogen stream (100 K) during the measurement.

Single-crystal X-ray diffraction data was collected at low temperature (100 K) on a Rigaku OD XtaLAB Synergy-S diffractometer equipped with a Dectris EIGER2 R CdTe 1M hybrid pixel array detector and an Oxford Cryosystems 800 Series Cryostream, using microfocused Ag *K*α radiation (λ = 0.56087 Å). *CrysAlisPro* software was employed for data processing, utilizing empirical and numerical absorption corrections.[30] All crystal structures were solved using *SUPERFLIP*[31] and refined with *SHELXL*[32] within *Olex2* software.[33] Figures were prepared using the *DIAMOND* software.[34]

2.5. Raman spectroscopy

Low-temperature Raman spectra were measured on a Bruker Senterra II confocal Raman microscope using a 785 nm laser. Spectra were measured in the 50–1410 cm^{-1} range with a spectral resolution of 1.5 cm^{-1} using a 15 × 1000 μm aperture. Measurements were performed at 100 K using a Linkam LTS420 low-temperature stage. Background subtraction was applied using three iterations of concave rubber-band correction with 64 baseline points, as implemented in the Bruker *OPUS 8.7* software suite. Prior to analysis, samples were loaded inside an inert-atmosphere glovebox into rigorously dried and F_2-passivated 500 μm quartz capillaries, which were then flame-sealed prior to measurement.

3. Results and discussion

3.1. Syntheses

Reaction of $n XeF_2 \cdot PtF_4$ ($1 < n < 1.6$) with an excess of XeF_2 at temperatures above the melting point of XeF_2 predictably resulted in oxidation of Pt^{IV} to Pt^{V},[19] and characterization of the resulting yellow solid identified it as a previously unobserved phase, [Xe_2F_3][PtF_6]·XeF_2(*mC*120) (eq 1).

$$n XeF_2 \cdot PtF_4 + (3.5 - n) XeF_2 \xrightarrow{130\ ^\circ C} [Xe_2F_3][PtF_6] \cdot XeF_2(mC120) + 0.5Xe \quad (1)$$

As previously reported, [Xe_2F_3][PtF_6] was the sole isolated product obtained following oxidation of PtF_4 with excess XeF_2 and subsequent removal of "unreacted" XeF_2 under vacuum.[19] This observation suggested that [Xe_2F_3][PtF_6]·XeF_2 undergoes loss of XeF_2 upon prolonged exposure to dynamic vacuum at room temperature. This hy-

pothesis was confirmed, as $[Xe_2F_3][PtF_6]$ readily formed when $[Xe_2F_3][PtF_6]\cdot XeF_2$ was subjected to dynamic vacuum for several hours (eq 2). The resulting poorly crystalline material could subsequently be recrystallized from aHF to afford yellow crystals suitable for structural characterization.

$$[Xe_2F_3][PtF_6]\cdot XeF_2 \xrightarrow{\text{dyn. vac.}} [Xe_2F_3][PtF_6] + XeF_2 \quad (2)$$

A second polymorph of $[Xe_2F_3][PtF_6]\cdot XeF_2$ was obtained from reactions in aHF solution employing an approximately threefold excess of XeF_2 relative to $RbPtF_6$. Its formation could be rationalized by partial displacement of the alkali metal as RbF, which is released into solution (eq 3).

$$3XeF_2 + RbPtF_6 \longrightarrow [Xe_2F_3][PtF_6]\cdot XeF_2(oP120) + RbF \quad (3)$$

All attempts to synthesize $[XeF][Pt_2F_{11}]$ in this work were unsuccessful. Crystallization from aHF solution at ambient temperature employing the targeted stoichiometry yielded only $[XeF][PtF_6](mP108)$ as large single crystals, accompanied by unreacted PtF_5. Likewise, heating a 1:2 mixture of XeF_2 and PtF_5 in a heat-sealed FEP ampoule at 70 °C produced the *mP*36 polymorph of $[XeF][PtF_6]$. Interestingly, the structure of $[XeF][PtF_6](mP108)$ was found to be related to that of $[XeF][IrF_6]$, which was likewise isolated from aHF solution,[14] whereas $[XeF][PtF_6]$ (*mP*36) appears to be structurally related to $[XeF][RuF_6]$, obtained by thermal reaction of XeF_2 with RuF_5.[13] These parallels suggest that polymorph selectivity in such systems is influenced by the employed synthetic approach.

Additionally, the synthesis of $[XeF][Pt_2F_{11}]$ was also attempted from aHF solutions containing XeF_2 and PtF_5 in an approximate 1:2.5 molar ratio, either by slow removal of the solvent at temperatures between −45 °C and −55 °C, or by gradual cooling of the solution to −60 °C. Furthermore, an attempt was made to react $[XeF][PtF_6]$ with a slight excess of PtF_5 at 65 °C, thus emulating the previously reported synthesis of $[XeF][Pt_2F_{11}]$ from $Xe(PtF_6)_2$.[18] None of these experiments yielded crystals of the targeted $[XeF][Pt_2F_{11}]$ compound, and no Raman bands unambiguously attributable to this phase were detected. Instead, only the presence of $[XeF][PtF_6]$ and unreacted PtF_5 were confirmed.

3.2. Single-crystal X-ray diffraction

The members of the XeF_2–PtF_5 system obtained in this work were structurally characterized by low-temperature (100 K) single-crystal X-ray diffraction. A summary of the crystallographic data is provided in Table 1, and selected bond distances and angles are listed in Table 2. Complete crystallographic parameters are compiled in the Supporting information (Tables S1–S6).

3.2.1. Crystal structures of $[Xe_2F_3][PtF_6]\cdot XeF_2(mC120)$ and $[Xe_2F_3][PtF_6]\cdot XeF_2(oP120)$

$[Xe_2F_3][PtF_6]\cdot XeF_2$ crystallizes in two polymorphs, namely in the monoclinic space group *C*2/*c* with Pearson symbol *mC*120 and in the orthorhombic space group *Pbca* with Pearson symbol *oP*120. Both structures feature eight formula units per unit cell ($Z = 8$) and one formula unit in the asymmetric unit ($Z' = 1$) and comprise well-separated $[Xe_2F_3]^+$ and $[PtF_6]^-$ ions together with cocrystallized XeF_2 molecules (Figures 2, 3). The two polymorphs differ, however, in their crystal packing (Figures S1, S2). Despite the established parallels between the XeF_2–PtF_5 and XeF_2–RuF_5 systems and the known isostructural relationship between [XeF]

Table 1. Summary of crystal data and refinement results.

Compound	$[Xe_2F_3][PtF_6]\cdot XeF_2(mC120)$	$[Xe_2F_3][PtF_6]\cdot XeF_2(oP120)$	$[Xe_2F_3][PtF_6]$	$[XeF][PtF_6](mP108)$
T (K)	100	100	100	100
Crystal system, space group	Monoclinic, *C*2/*c*	Orthorhombic, *Pbca*	Monoclinic, *Ia*	Monoclinic, $P2_1/n$
a (Å)	15.82016(16)	8.99866(8)	10.8860(2)	7.91407(6)
b (Å)	9.44604(9)	13.29342(14)	8.09069(16)	10.79245(8)
c (Å)	15.56492(16)	18.61809(18)	9.82822(19)	21.17145(16)
β (°)	109.7185(12)	90	92.1157(16)	91.6071(7)
V (Å^3)	2189.60(4)	2227.15(4)	865.03(3)	1807.59(2)
Z	8	8	4	12
M_w (g mol^{-1})	797.99	797.99	628.69	459.39
D_{calcd} (g cm^{-3})	4.841	4.760	4.827	5.064
μ (mm^{-1})	11.85	11.65	12.93	15.60
R_1	0.027	0.020	0.036	0.023
wR_2	0.070	0.039	0.094	0.052
S	1.044	1.043	1.076	1.026
$\Delta\rho_{min}$, $\Delta\rho_{max}$ (e Å^{-3})	−4.08, 2.46	−1.05, 1.53	−1.36, 2.35	−2.91, 2.28

Table 2. Selected bond distances (Å) and angles (°).

	$[Xe_2F_3][PtF_6]\cdot XeF_2$(*mC*120)	$[Xe_2F_3][PtF_6]\cdot XeF_2$(*oP*120)	$[Xe_2F_3][PtF_6]$	[XeF][PtF_6](*mP*108)
Xe–F [a]	1.9779(12), 1.9993(12)	1.9855(12), 1.9900(13)		
Xe–F_t [b]	1.9118(12), 1.9133(12)	1.9187(13), 1.9232(12)	1.914(9), 1.917(9)	
Xe–F_b(Xe)	2.1690(12), 2.1825(12)	2.1612(12), 2.1757(12)	2.143(9), 2.143(9)	
Xe–F_t [c]				1.8934(16)–1.9023(15)
Xe–F_b(Pt)				2.2255(14)–2.2741(14)
Pt–F_t	1.8771(13)–1.8909(13)	1.8744(12)–1.8871(12)	1.877(7)–1.894(9)	1.8637(14)–1.8809(13)
Pt–F_b				1.9552(14)–1.9590(14)
F–Xe–F [a]	178.48(6)	179.23(6)		
F–Xe–F [b]	178.75(5), 179.28(5)	177.05(6), 178.16(5)	176.6(4), 178.7(4)	
F–Xe–F [c]				175.97(7)–179.26(7)
Xe–F_b–Xe	136.77(6)	134.03(6)	158.2(4)	
Pt–F–Xe				117.33(6)–138.42(8)
cis-F–Pt–F	89.11(7)–90.86(7)	89.65(6)–90.79(6)	88.6(4)–91.4(4)	87.87(7)–91.96(7)
trans-F–Pt–F	179.89(8)–179.97(7)	179.41(6)–179.63(6)	179.0(5)–179.1(4)	177.72(8)–179.74(9)

[a] cocrystallized XeF_2 molecule; [b] $[Xe_2F_3]^+$ cation; [c] XeF_2 molecule bound to Pt^V center; F_t: terminal, F_b: bridging.

$[RuF_6]$ and [XeF][PtF_6],[3,13,18] neither of the two polymorphic forms of $[Xe_2F_3][PtF_6]\cdot XeF_2$ is isostructural with the previously structurally characterized $[Xe_2F_3][RuF_6]\cdot XeF_2$.[15]

The V-shaped $[Xe_2F_3]^+$ cations display among the least obtuse Xe–F–Xe angles reported for this motif to date (136.77(6)° in *mC*120; 134.03(6)° in *oP*120) (Table 2),[9,15,35,36] and are markedly more closed than the corresponding angle in $[Xe_2F_3][RuF_6]\cdot XeF_2$ (154.3(4)°).[15] In neither polymorph is the cation perfectly symmetric, as the two longer Xe–F_b distances are unequal (2.1690(12), 2.1825(12) Å in *mC*120; 2.1612(12), 2.1757(12) Å in *oP*120), whereas the shorter Xe–F_t bonds do not differ significantly (1.9118(12), 1.9133(12) Å in *mC*120; 1.9187(13), 1.9232(12) Å in *oP*120). The F–Xe–F angles within the $[Xe_2F_3]^+$ cations deviate only slightly from linearity (178.75(5), 179.28(5)° in *mC*120; 177.05(6), 178.16(5)° in *oP*120).

In both structures, the fluorine coordination environment around the Pt^V centers deviates only marginally from ideal octahedral (O_h) symmetry. The Pt–F bond lengths span comparable ranges in the two polymorphs (1.8771(13)–1.8909(13) Å in *mC*120; 1.8744(12)–1.8871(12) Å in *oP*120), and the *cis*- and *trans*-F–Pt–F angles remain close to those expected for an octahedral environment (89.11(7)–90.86(7) and 179.89(8)–179.97(7) in *mC*120; 89.65(6)–90.79(6)° and 179.41(6)–179.63(6)° in *oP*120). The observed Pt–F distances are in good agreement with those reported for previously characterized salts containing discrete $[PtF_6]^-$ anions.[27,37,38]

The cocrystallized XeF_2 molecules adopt a geometry close to the ideal linear, centrosymmetric $D_{\infty h}$ arrangement observed in the crystal structure of XeF_2. The observed Xe–F bond distances (1.9779(12), 1.9994(12) Å in *mC*120; 1.9855(12), 1.9900(13) Å in *oP*120) are in good agreement with the Xe–F bond distance reported for XeF_2 (1.999(4) Å),[12] and the F–Xe–F angles remain nearly linear (178.48(6)° in *mC*120; 179.23(6)° in *oP*120).

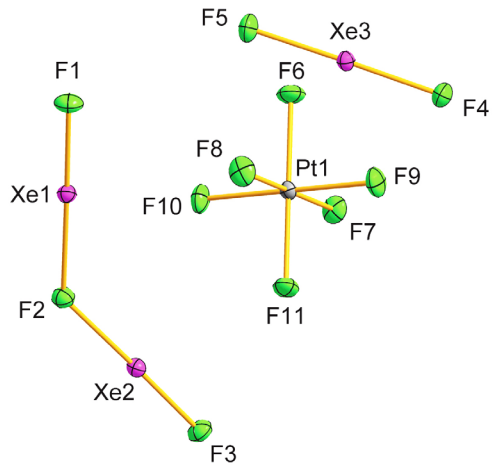

Figure 2. Asymmetric unit of $[Xe_2F_3][PtF_6]\cdot XeF_2$(*mC*120), showing atom labeling. Ellipsoids are drawn at the 50% probability level.

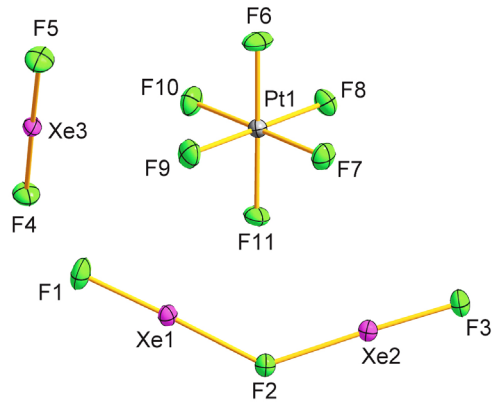

Figure 3. Asymmetric unit of $[Xe_2F_3][PtF_6]\cdot XeF_2$(*oP*120), showing atom labeling. Ellipsoids are drawn at the 50% probability level.

3.2.2 Crystal structure of $[Xe_2F_3][PtF_6]$

$[Xe_2F_3][PtF_6]$ crystallizes in the monoclinic space group *Ia* (Z = 4, Z' = 1) and comprises discrete $[Xe_2F_3]^+$ and $[PtF_6]^-$ ions (Figure 4). The compound is isostructural with the previously structurally characterized $[Xe_2F_3][RuF_6]$ and $[Xe_2F_3][IrF_6]$; however, an *Ia* setting was chosen for $[Xe_2F_3][PtF_6]$ instead of *Cc*, which was used for the Ru and Ir analogues.[15] This choice affords a monoclinic angle β (92.116(2)°), which is substantially closer to 90°,[39] than the values reported for $[Xe_2F_3][RuF_6]$ (136.825(6)°) and $[Xe_2F_3][IrF_6]$ (136.954(7)°).[15]

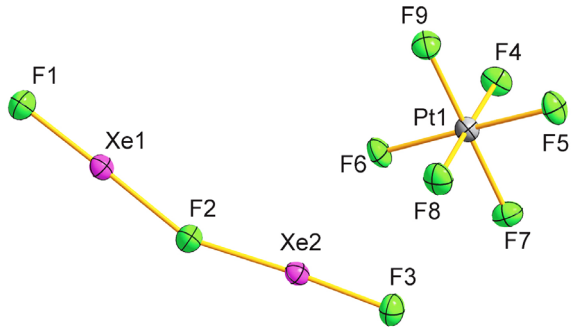

Figure 4. Asymmetric unit of $[Xe_2F_3][PtF_6]$, showing atom labeling. Ellipsoids are drawn at the 50% probability level.

The Xe–F–Xe angle (158.2(4)°) in the $[Xe_2F_3]^+$ cation is markedly more open than in the $[Xe_2F_3][PtF_6]\cdot XeF_2$ structures, albeit slightly less so than in the related $[Xe_2F_3][RuF_6]$ (161.5(5)°) and $[Xe_2F_3][IrF_6]$ (161.3(8)°). Within experimental uncertainty, the two Xe–F_b distances are equivalent (2.143(9), 2.143(9) Å), as are the two Xe–F_t bonds (1.914(9), 1.917(9) Å). The $[PtF_6]^-$ anion exhibits only minor deviations from octahedral geometry, as reflected in *cis*- and *trans*-F–Pt–F angles (88.6(4)–91.4(4)° and 179.0(5)–179.1(4)°, respectively). The Pt–F bond lengths (1.877(7)–1.894(9) Å) fall in the same range as those observed in the $[Xe_2F_3][PtF_6]\cdot XeF_2$ structures.

3.2.3. Crystal structure of $[XeF][PtF_6]$(*mP*108)

$[XeF][PtF_6]$(*mP*108) crystallizes in the monoclinic space group $P2_1/n$ and contains three crystallographically independent $[XeF][PtF_6]$ tight ion pairs in the asymmetric unit (Z' = 3) (Figure 5). Its unit-cell parameters closely resemble those reported for $[XeF][IrF_6]$, although the structure of the Ir analogue was reported in the $P2_1/c$ space group.[14]

The XeF_2 units bound to the Pt^V center retain a nearly linear F–Xe–F geometry (175.97(7)–179.26(7)°) but exhibit a pronounced asymmetry in their Xe–F bond lengths, characterized by elongation of the bridging Xe–F_b bonds (2.2255(14)–2.2741(14) Å) accompanied by contraction of the terminal Xe–F_t bonds (1.8934(16)–1.9023(15) Å), indicative of ionization of XeF_2 along the $XeF_2 \rightarrow XeF^+ + F^-$ pathway.[40] The Xe–F_b bond lengths closely match those

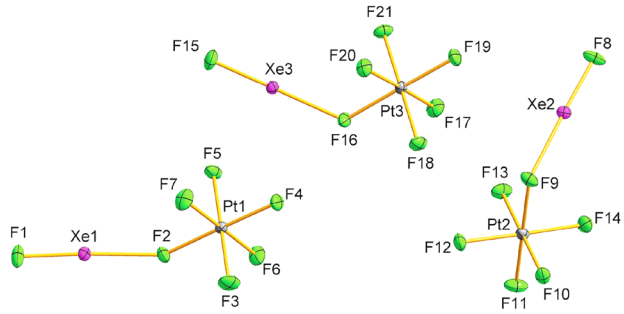

Figure 5. Asymmetric unit of $[XeF][PtF_6]$, featuring the three symmetry-inequivalent units and showing atom labeling. Ellipsoids are drawn at the 50% probability level.

reported for $[XeF][IrF_6]$ (2.220(4)–2.272(4) Å), whereas the corresponding Xe–F_t bonds in the Ir analogue are appreciably shorter (1.854(5)–1.867(5) Å).[14] The Pt–F–Xe angles within the three crystallographically independent moieties vary substantially (117.33(6), 124.20(7), and 138.42(8)°), closely matching those reported for $[XeF][IrF_6]$ (119.3–141.9°). The smallest value represents the least obtuse A–F–Xe angle observed in a $[XeF][AF_6]$ structure to date.[12–14]

The Pt–F_b bond lengths (1.9552(14)–1.9590(14) Å) are notably elongated relative to Pt–F_t bonds (1.8637(14)–1.8809(13) Å), the latter being comparable to those observed for discrete $[PtF_6]^-$ anions characterized in this work. Nevertheless, the coordination environment of Pt^V remains close to octahedral, as reflected by *cis*- and *trans*-F–Pt–F angles (87.87(7)–91.96(7)° and 177.72(8)–179.74(9)°, respectively).

3.2.4. Crystal structure of $[XeF][PtF_6]$(*mP*36)

Crystals of $[XeF][PtF_6]$(*mP*36) were of poor quality and yielded only low-resolution diffraction data, precluding a detailed structural analysis. Consequently, only the unit-cell parameters could be determined (a = 7.0440(4), b = 10.8225(5), c = 7.9242(4), β = 91.212(5), V = 603.96(5), Z' = 1, space group $P2_1/n$). These closely resemble both the parameters derived from PXRD data[18] and those reported for $[XeF][RuF_6]$ (with the a and c axes interchanged),[13] corroborating earlier observations based on PXRD patterns that the two compounds are isostructural.[18]

3.3. Raman spectroscopy

Low-temperature (100 K) Raman spectra of the two polymorphs of $[Xe_2F_3][PtF_6]\cdot XeF_2$, $[Xe_2F_3][PtF_6]$, and $[XeF][PtF_6]$(*mP*108) are shown in Figure 6, with peak positions and relative intensities tabulated in the Supporting Information (Table S7).

The Raman spectra of both $[Xe_2F_3][PtF_6]\cdot XeF_2$ polymorphs exhibit their most intense features in the region attributable to the symmetric and asymmetric Xe–F_t stretching modes of the $[Xe_2F_3]^+$ cation (580–598 cm^{-1}).[9]

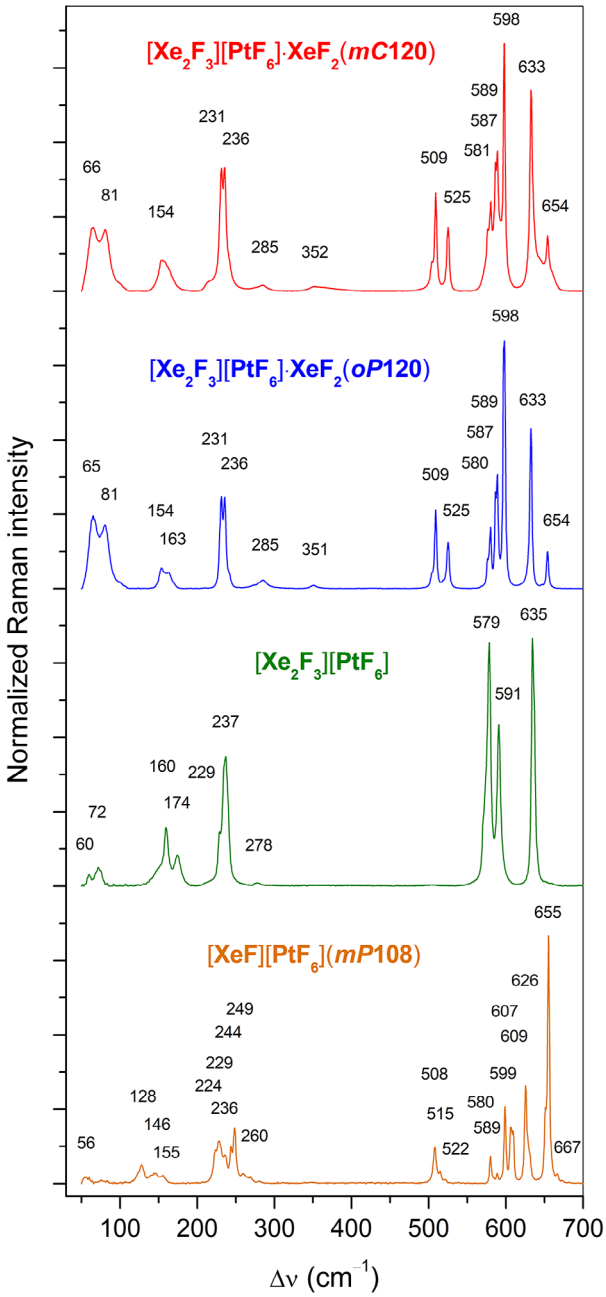

Figure 6. Low-temperature (100 K) Raman spectra of $[Xe_2F_3][PtF_6]{\cdot}XeF_2$(*mC*120), $[Xe_2F_3][PtF_6]{\cdot}XeF_2$(*oP*120), $[Xe_2F_3][PtF_6]$, and $[XeF][PtF_6]$(*mP*108).

Bands associated with the $[PtF_6]^-$ anion, corresponding to the ν_1 (633, 654 cm^{-1}) and ν_5 (231, 236 cm^{-1}) modes, are likewise readily identified.[19,27] The presence of cocrystallized XeF_2 is reflected by two medium-intensity bands (509, 525 cm^{-1}). Corresponding bands were also reported in the ambient-temperature spectra of the Ru (506, 515 cm^{-1}) and Ir (506, 516 cm^{-1}) analogues.[15] Overall, the spectra of the *mC*120 and *oP*120 polymorphs are nearly identical.

The low-temperature Raman spectra of $[Xe_2F_3][PtF_6]$ and $[XeF][PtF_6]$(*mP*108) recorded in this work are also consistent, in terms of the positions of their strongest bands, with previously reported ambient-temperature spectra of these compounds.[3,19]

4. Conclusions

Reexploration of the XeF_2–PtF_5 system has resulted in the synthesis of the novel compound $[Xe_2F_3][PtF_6]{\cdot}XeF_2$, along with $[Xe_2F_3][PtF_6]$ and $[XeF][PtF_6]$, all of which were characterized by SCXRD and Raman spectroscopy. Both $[Xe_2F_3][PtF_6]{\cdot}XeF_2$ and $[XeF][PtF_6]$ were found to occur in two polymorphs, with polymorph selectivity apparently depending on the synthetic approach employed. In the low-temperature Raman spectra of the $[Xe_2F_3][PtF_6]{\cdot}XeF_2$ phases, main bands attributable to the constituent moieties could be readily assigned, whereas the spectra of $[Xe_2F_3][PtF_6]$ and $[XeF][PtF_6]$(*mP*108) are consistent with literature data. Collectively, these results provide the first crystallographically characterized representatives of the XeF_2–PtF_5 family and expand the set of structurally elucidated phases formed by interaction of XeF_2 with strongly Lewis-acidic pentafluorides.

Supplementary material

Additional crystallographic data, figures, and a table listing the observed Raman band positions with their relative intensities are provided in the Supporting Information. Supplementary crystallographic data (CIF files) may be obtained free of charge from FIZ Karlsruhe via www.ccdc.cam.ac.uk/structures by quoting the depository numbers CSD 2529289 ($[Xe_2F_3][PtF_6]{\cdot}XeF_2$(*mC*120)), 2529288 ($[Xe_2F_3][PtF_6]{\cdot}XeF_2$(*oP*120)), 2529287 ($[Xe_2F_3][PtF_6]$), and 2529290 ($[XeF][PtF_6]$(*mP*108)). Full experimental data for this article, including SCXRD datasets and Raman spectra, is available from the Zenodo open repository at https://doi.org/10.5281/zenodo.18428037.

Acknowledgements

The authors gratefully acknowledge the financial support from the Slovenian Research and Innovation Agency (ARIS) (N1-0189, N1-0225), the European Research Council (ERC) under the European Union's Horizon 2020 Research and Innovation Programme (Starting Grant No. 950625), and the Jožef Stefan Institute Director's Fund.

5. References

1. M. Tramšek, B. Žemva, *Acta Chim. Slov.* **2006**, *53*, 105–116.
2. F. O. Sladky, P. A. Bulliner, N. Bartlett, B. G. DeBoer, A. Zalkin, *Chem. Commun. (London)* **1968**, 1048–1049. **DOI:**10.1039/c19680001048

3. F. O. Sladky, P. A. Bulliner, N. Bartlett, *J. Chem. Soc. A* **1969**, 2179–2188. **DOI:**10.1039/J19690002179
4. B. Žemva, J. Slivnik, *J. Inorg. Nucl. Chem.* **1971**, *33(11)*, 3952–3953. **DOI:**10.1016/0022-1902(71)80304-4
5. R. J. Gillespie, B. Landa, *Inorg. Chem.* **1973**, *12(6)*, 1383–1389. **DOI:**10.1021/ic50124a034
6. B. Frlec, J. H. Holloway, *J. Chem. Soc., Dalton Trans.* **1975**, 535–540. **DOI:**10.1039/DT9750000535
7. J. H. Holloway, G. J. Schrobilgen, *J. Chem. Soc., Chem. Commun.* **1975**, 623–624. **DOI:**10.1039/C39750000623
8. B. Žemva, *Croat. Chem. Acta* **1988**, *61(1)*, 163–187.
9. B. A. Fir, M. Gerken, B. E. Pointner, H. P. A. Mercier, D. A. Dixon, G. J. Schrobilgen, *J. Fluorine Chem.* **2000**, *105(1)*, 159–167. **DOI:**10.1016/S0022-1139(00)00306-7
10. J. Burgess, C. J. W. Fraser, V. M. McRae, R. D. Peacock, D. R. Russell, *J. Inorg. Nucl. Chem.* **1976**, *28*, 183–188. **DOI:**10.1016/0022-1902(76)80624-0
11. A. Zalkin, D. L. Ward, R. N. Biagioni, D. H. Templeton, N. Bartlett, *Inorg. Chem.* **1978**, *17(5)*, 1318–1322. **DOI:**10.1021/ic50183a044
12. H. St. A. Elliott, J. F. Lehmann, H. P. A. Mercier, H. D. B. Jenkins, G. J. Schrobilgen, *Inorg. Chem.* **2010**, *49(18)*, 8504–8523. **DOI:**10.1021/ic101152x
13. N. Bartlett, M. Gennis, D. D. Gibler, B. K. Morrell, A. Zalkin, *Inorg. Chem.* **1973**, *12(8)*, 1717–1721. **DOI:**10.1021/ic50126a002
14. F. Tamadon, S. Seidel, K. Seppelt, *Acta Chim. Slov.* **2013**, *60(3)*, 491–494.
15. M. Tramšek, E. Goreshnik, G. Tavčar, *Acta Chim. Slov.* **2016**, *63(2)*, 369–375. **DOI:**10.17344/acsi.2016.2373
16. N. Bartlett, *Proc. Chem. Soc.* **1962**, 218. **DOI:**10.1039/ps9620000197
17. N. Bartlett, N. K. Jha, in: H. H. Hyman (Ed.): Noble-gas compounds, The University of Chicago Press, Chicago, **1963**, pp. 23–30.
18. L. Graham, O. Graudejus, N. K. Jha, N. Bartlett, *Coord. Chem. Rev.* **2000**, *197(1)*, 321–334. **DOI:**10.1016/S0010-8545(99)00190-3
19. N. Bartlett, B. Žemva, L. Graham, *J. Fluorine Chem.* **1976**, *7(1–3)*, 301–320. **DOI:**10.1016/S0022-1139(00)84003-8
20. D. Peters, R. Miethchen, *J. Fluorine Chem.* **1996**, *79(2)*, 161–165. **DOI:**10.1016/S0022-1139(96)03484-7
21. E. B. Segal, *Chem. Health Saf.* **2000**, *7(1)*, 18–23. **DOI:**10.1016/S1074-9098(99)00077-5
22. M. Möbs, F. Kraus, *ACS Chem. Health Saf.* **2025,** *32(5),* 662–672. **DOI:**10.1021/acs.chas.5c00117
23. K. Motaln, K. Gurung, P. Brázda, A. Kokalj, K. Radan, M. Dragomir, B. Žemva, L. Palatinus, M. Lozinšek, *ACS Cent. Sci.* **2024**, *10(9)*, 1733–1741. **DOI:**10.1021/acscentsci.4c00815
24. M. Lozinšek, E. Goreshnik, B. Žemva, *Z. Anorg. Allg. Chem.* **2012**, *638(12–13)*, 2123–2128. **DOI:**10.1002/zaac.201200176
25. A. Šmalc, K. Lutar, in: R. N. Grimes (Ed.): Inorganic Syntheses, John Wiley & Sons, **1992**, *29,* pp. 1–4. **DOI:**10.1002/9780470132609.ch1
26. W. E. Falconer, G. R. Jones, W. A. Sunder, M. J. Vasile, A. A. Muenter, T. R. Dyke, W. Klemperer, *J. Fluorine Chem.* **1974**, *4(2)*, 213–234. **DOI:**10.1016/S0022-1139(00)82515-4
27. Z. Mazej, E. Goreshnik, K. O. Christe, *J. Fluorine Chem.* **2023**, *268*, 110128. **DOI:**10.1016/j.jfluchem.2023.110128
28. T. Drews, D. Rusch, S. Seidel, S. Willemsen, K. Seppelt, *Chem. Eur. J.* **2008**, *14(14)*, 4280–4286. **DOI:**10.1002/chem.200701786
29. K. Motaln, K. Gurung, M. Dragomir, D. Kurzydłowski, L. Palatinus, M. Lozinšek, *Inorg. Chem.* **2025**, *64(29)*, 14968–14976. **DOI:**10.1021/acs.inorgchem.5c01740
30. Rigaku OD, CrysAlisPro, Rigaku Corporation, Wrocław, Poland, **2025.**
31. L. Palatinus, G. Chapuis, *J. Appl. Crystallogr.* **2007**, *40(4)*, 786–790. **DOI:**10.1107/S0021889807029238
32. G. M. Sheldrick, *Acta Crystallogr. C* **2015**, *71(1)*, 3–8. **DOI:**10.1107/S2053229614024218
33. O. V. Dolomanov, L. J. Bourhis, R. J. Gildea, J. A. K. Howard, H. Puschmann, *J. Appl. Crystallogr.* **2009**, *42(2)*, 339–341. **DOI:**10.1107/S0021889808042726
34. H. Putz, K. Brandenburg, Diamond – Crystal and Molecular Structure Visualization, Crystal Impact, Bonn, Germany, **2025.**
35. K. Radan, E. Goreshnik, B. Žemva, *Angew. Chem Int. Ed.* **2014**, *53(50)*, 13715–13719. **DOI:**10.1002/anie.201406404
36. K. Motaln, M. Virant, M. Lozinšek, *Inorg. Chem.* **2026**, *65.* **DOI:**10.1021/acs.inorgchem.5c05940
37. O. Graudejus, B. G. Müller, *Z. Anorg. Allg. Chem.* **1996**, *622(6)*, 1076–1082. **DOI:**10.1002/zaac.19966220623
38. O. Graudejus, A. P. Wilkinson, L. C. Chacón, N. Bartlett, *Inorg. Chem.* **2000**, *39(13)*, 2794–2800. **DOI:**10.1021/ic000041w
39. A. D. Mighell, *Acta Crystallogr. B* **2003**, *59(2)*, 300–302. **DOI:**10.1107/S0108768103002829
40. B. Žemva, A. Jesih, D. H. Templeton, A. Zalkin, A. K. Cheetham, N. Bartlett, *J. Am. Chem. Soc.* **1987**, *109(24)*, 7420–7427. **DOI:**10.1021/ja00258a028

Povzetek

Sistem XeF_2–PtF_5 je bil ponovno raziskan s preučevanjem reakcij, ki so potekale v brezvodnem HF ali pri povišanih temperaturah. Ta pristop je omogočil strukturno karakterizacijo štirih predstavnikov sistema, in sicer $[Xe_2F_3][PtF_6]\cdot XeF_2$(*mC*120), $[Xe_2F_3][PtF_6]\cdot XeF_2$(*oP*120), $[Xe_2F_3][PtF_6]$ in $[XeF][PtF_6]$(*mP*108), z uporabo rentgenske difrakcije na monokristalu in nizkotemperaturne ramanske spektroskopije.